JOURNAL OF AGRICULTURAL AND FOOD CHEMISTRY

Article

pubs.acs.org/JAFC

Biofilms Benefiting Plants Exposed to ZnO and CuO Nanoparticles Studied with a Root-Mimetic Hollow Fiber Membrane

Michelle Bonebrake,[†] Kaitlyn Anderson,[†] Jonathan Valiente,[†] Astrid Jacobson,[‡] Joan E. McLean,[§] Anne Anderson,[∥] and David W. Britt*[,†]

[†]Department of Biological Engineering, Utah State University, Logan, Utah 84322, United States

[‡]Plants Soils Climate, Utah State University, Logan, Utah 84322, United States

[§]Utah Water Research Laboratory, Utah State University, Logan, Utah 84322, United States

[∥]Department of Biology, Utah State University, Logan, Utah 84322, United States

Supporting Information

ABSTRACT: Plants exist with a consortium of microbes that influence plant health, including responses to biotic and abiotic stress. While nanoparticle (NP)−plant interactions are increasingly studied, the effect of NPs on the plant microbiome is less researched. Here a root-mimetic hollow fiber membrane (HFM) is presented for generating biofilms of plant-associated microbes nurtured by artificial root exudates (AREs) to correlate exudate composition with biofilm formation and response to NPs. Two microbial isolates from field-grown wheat, a bacillus endophyte and a pseudomonad root surface colonizer, were examined on HFMs fed with AREs varying in N and C composition. Bacterial morphology and biofilm architecture were characterized using scanning electron microscopy (SEM) and atomic force microscopy (AFM) and responses to CuO and ZnO NP challenges of 300 mg/L evaluated. The bacillus isolate sparsely colonized the HFM. In contrast, the pseudomonad formed robust biofilms within 3 days. Dependent on nutrient sources, the biofilm cells produced extensive extracellular polymeric substances (EPS) and large intracellular granules. Pseudomonad biofilms were minimally affected by ZnO NPs. CuO NPs, when introduced before biofilm maturation, strongly reduced biofilm formation. The findings demonstrate the utility of the HFM root-mimetic to study rhizoexudate influence on biofilms of root-colonizing microbes but without active plant metabolism. The results will allow better understanding of how microbe-rhizoexudate−NP interactions affect microbial and plant health.

KEYWORDS: *nanoparticles, rhizosphere, microbiome, extracellular polymeric material, root mimetic*

INTRODUCTION

Plants have coevolved with soil microbes, forming a complex interkingdom relationship that helps each survive in the face of numerous abiotic and biotic stressors.[1,2] Endophytic microbes, initially existing within the seeds, may provide seedlings with a microbiome that becomes complimented by exogenous microbes from the environment. Microbial populations are higher in the root zone through the secretions of metabolites by root cells, the process of rhizoexudation, and the release of border cells from the root cap.[3] The resulting boundary layer, the rhizosphere, is richer in sugars, amino acids, organic acids, and other secondary metabolites than the soil pore water.[4,5] Depending on the plant species, developmental stage, and environmental conditions, plants may release as high as 40% of the total carbon fixed through photosynthesis in root exudates.[6,7] The actual input of C into the soil as exudates is uncertain, but this enrichment of the organic content of the rhizosphere establishes a microcosm with composition and functions that are influenced by the plant.[2,8] Bacterial colonization of roots, through biofilm formation, is one of the consequences.[9,10]

This is not, however, a one-way relationship. The plant microbiome influences plant health through a variety of mechanisms that provide protection against biotic and abiotic stress.[11,12] Beneficial microbes, such as the bacterial root colonizer, *Pseudomonas chlororaphis* O6 (*Pc*O6), produce antimicrobials that aid in protection against pathogens.[13] Other metabolites modulate plant functions, including closure of stomates by the volatile butanediol, a process contributing to drought protection.[14] Also, iron in the rhizosphere is routed to the bacteria and plant but can be restricted from pathogenic microbes, through microbial secretion of highly effective, metal-chelating siderophores.[15,16] This feedback loop between bacteria and plant is mutually beneficial. Thus, the multitude of external factors that directly influence one will, likely through indirect pathways, influence the other.

It is becoming increasingly recognized that maintaining, and even augmenting, the plant microbiome will be necessary for sustainable agricultural output to keep pace with growing demand.[17,18] To further optimize agricultural output, next generation fertilizers and pesticides are being explored, with targeted and timed delivery through nanoformulations.[19] Some of the fertilizer applications may supply the nutrients directly, whereas others may be indirect. For instance, applications of

Special Issue: Nanotechnology Applications and Implications of Agrochemicals toward Sustainable Agriculture and Food Systems

Received: May 31, 2017
Revised: September 11, 2017
Accepted: September 19, 2017
Published: September 19, 2017

DOI: 10.1021/acs.jafc.7b02524
J. Agric. Food Chem. 2018, 66, 6619−6627

TiO_2 or Fe_3O_4 NPs may enhance P supply through acidification of the rhizosphere caused by NP challenge.[20] Another mechanism associated with ZnO NP treatments that increase plant P involves stimulation of phosphatase activity in microbes through Zn release from dissolution of the NPs, the resulting Zn phosphate acting as a source of P.[21] As these formulations are developed, model systems for studying rhizosphere processes are required to assess the interplay between the root, beneficial microbes, and external agents such as NPs as illustrated in Figure 1.

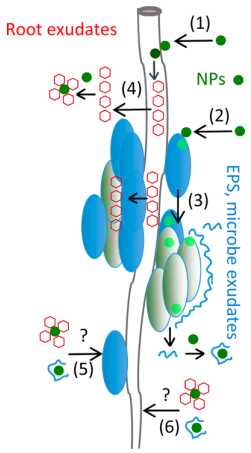

Figure 1. NPs arriving at the microbially colonized root may directly adsorb to/enter the root (1) and bacteria (2). NP−microbe interactions alter colonization, metabolite production, biofilm formation, and architecture (3). NP−root interactions influence root metabolite production and exudation (4). In turn, NP remodeling and biocoating may result, potentially altering NP bioactivity (5, 6). Not depicted: Endophytic microbes within the root tissues, NP-released ions, and components from soil pore waters that will influence NP fate and bioavailability.

Hydroponic growth of plants affords a detailed focus on the NP−plant interactions, revealing the uptake and translocation of NPs; for instance, CuO NPs travel through roots, into foliar tissues, and return to the roots.[22] Thus, hydroponic systems provide key insights in terms of NP fate and translocation and plant cell responses under model conditions. Studies of NP influence on root-colonizing microbes also often take a similar reductionist approach, investigating NP−microbe interactions with planktonic microbes.[23,24] Findings relevant to toxicity of distinct classes of engineered NPs are gained. However, bacteria associated with the root surface exist not only as planktonic cells but are embedded in a matrix termed the biofilm. Biofilm growth confers resistance to many environmental challenges such as antibiotics.[25] It also provides the microbes direct access to the rhizoexudates and, in return, bacterial metabolites are concentrated in the root zone, intensifying their influence on the plant or other rhizosphere organisms. Thus, studies under conditions of hydroponic plant growth or with planktonic cells do not duplicate the environment of the rhizosphere as established in agricultural soils.

To study the influence of root exudates on soil microbial communities, root-models have been developed to focus on the biofilm lifestyle of rhizosphere microbes. Root-colonizing bacteria such as *Pc*O6 form biofilms on synthetic surfaces, including polystyrene well plates in several media.[26] In contrast, a plant-beneficial *Burkholderia* isolate from sugar cane only forms biofilms in well plates containing growth medium amended with metabolites prepared from macerated sugar cane roots.[27] An *in situ* platform functioning as a root-mimetic was developed by Ziegler et al., in which thin agar films containing artificial root exudates (AREs) are deposited on glass slides, that when placed in soil allow bacteria that metabolize the AREs to be detected.[28] A continuous ARE-delivery artificial root was developed in which a rolled filter paper wick delivers nutrients into soil samples to assess changes in soil microbial composition as a function of carbon loading and distance from the wick. This method has also been used to augment the rhizosphere with AREs to assess the role of specific metabolites, such as 8-hydroxyquinoline, a potential allelochemical from knapweed, on microbial community composition in native soil.[29] The filter paper wicks are conduits to deliver AREs into the soil and, as such, are not actual root-mimetics for assessing biofilm formation and response to ARE changes and/or external challenges.

Here, we employ hollow fiber membranes (HFM) as root-mimetics for assessing biofilm growth as a function of ARE composition and NP challenges. NP interactions with root-colonizing microbes on living roots are complex as the response of the root to the NP challenge (whether directly or through NP-induced alteration in rhizosphere metabolite production) convolutes the situation as depicted in Figure 1. Surface-sterilization of seeds and planting into sterilized growth matrix such as sand are employed to study the NP−plant interactions without bacterial contributions. However, to study the root-colonizing microbe as a biofilm, without influence from active plant metabolism, a model system such as a hemodialysis hollow fiber membrane (HFM), can be used to deliver isolated root exudates, or ARE, either through the lumen or externally. HFMs, developed for dialysis and ultrafiltration, can be applied as bioinert surfaces for culturing biofilms. Microbial trapping *within* HFMs has been used to stimulate growth of "unculturable" bacteria by reintroduction into soils, where the soil pore waters carrying the nutrients flow across the fiber walls stimulate growth.[30] This system can be placed in the rhizosphere where it functions as a permeable-selective cell encapsulation platform for cell culture as an *in situ* HFM bioreactor.

The high-flux PS/PVP HFM fiber is evaluated here as root-mimetic where microbes colonize the outer surface, allowing for facile analysis of soil microbe biofilm formation as a function of ARE composition and in response to external challenges of engineered NPs. We have previously established that *P. chlororaphis* O6 (*Pc*O6) colonizes the root surfaces of seedlings at densities that are not impaired by growth in sand amended with CuO or ZnO NPs[31,32] and attribute their survival to the formation of the protectant biofilms on the root surface. Isolates of *Bacillus subtilis* are strong biofilm formers and also have biocontrol activity for the plant.[33] The *B. subtilis* endophyte used in these studies, designated as *Bs*309, was from surface-sterilized commercial wheat seeds. Distinct biofilm forming abilities of the two microbes on the HFMs are demonstrated and correlations between ARE composition, biofilm architecture, and cell morphologies are observed. Challenges of CuO or ZnO NPs delivered at different time points reveal differential impacts on bacterial cell morphology and biofilm formation.

DOI: 10.1021/acs.jafc.7b02524
J. Agric. Food Chem. 2018, 66, 6619−6627

MATERIALS AND METHODS

Hollow Fiber Membranes. HFMs of PS/PVP, PS, and cellulose diacetate (CD) were obtained from Fresenius Medical Care North America, Ogden, UT. Bleach-treated PS/PVP HFMs were prepared in 0.57% sodium hypochlorite at 70 °C for 2 min and rinsed 3× in double distilled water. The bleach-treatment is a facile means to reduce the PVP content of the fiber, creating a membrane whose properties can be tuned between those of PS/PVP and pure PS.[34] The HFMs have lumen diameters <200 μm and wall thickness <50 μm, and molecular weight (MW) cutoff <60 kDa.

Artificial Root Exudate (ARE) Formulations. All of the chemicals used were of analytical grade and were obtained from either Sigma-Aldrich or Fisher Scientific. Five different media recipes were utilized as AREs to deliver nutrients to the bacteria: Luria Broth, LB, (ARE A); minimal medium (ARE B); ARE B with glycine, ARE B(+gly); ARE B with additional citrate, ARE B(+cit); and ARE B with glycine and additional citrate ARE B(+gly,+cit). Specific ARE recipes can be found in the Supporting Information as Table S1. ARE A and ARE B both support *Pc*O6 biofilm formation.[26]

Nanoparticle Source. Commercially available CuO (nominal particle size <50 nm) and ZnO (<100 nm) (Sigma-Aldrich Co.) powders were used in this study and have been previously characterized in 2012 for size and elemental purity.[15] The NP powders were protected from light and used as-received, without further characterization prior to use. NP size and morphology observed here with SEM (Supporting Information) are consistent with prior characterization. NP solutions of 2.1 mg metal/mL in double distilled deionized (DDI) water were vortex mixed and placed in a sonication bath for 5 min just before use.

Wheat Growth. Wheat, cultivar *Doloris*, was grown in a sterile sand matrix as previously described.[31,32] Fresh wheat roots from 7 days-seedlings grown in sand were carefully extracted from the sand, rinsed in sterile DDI water, and mounted on glass slides for AFM and optical microscopy analysis. For SEM, imaging samples were chemically fixed in methanol, critical point dried, and mounted on copper tape.

Microbial Growth. Bacterial cultures (*Pc*O6 and *Bs*309) were maintained as frozen stocks at −70 °C in 15% sterile glycerol. To obtain inoculum, cells from the thawed freezer stocks were inoculated into either ARE A or B and grown for 24 or 48 h in darkness at 22 °C with shaking at 150 rpm in a series 25 incubator shaker (New Brunswick Scientific Co., Edison, NJ).

Biofilm Development and Nanoparticle Challenges. Biofilm generation on the outside of the HFMs was assessed by draping fibers into the wells of a 12-well plate (Nunclon Delta Surface, Fisher Scientific Co.) and affixing the free ends to the top of the plate. AREs were added to the wells (3 mL/well) followed by 2 μL of inoculum containing 1 × 10^6 cells/mL and incubated at 22 °C at 150 rpm. Freshly prepared NP stock solutions were vortex mixed for 5 min then added either at the same time as the inoculum (0 h) or 3 days after inoculation to select wells containing the HFMs with biofilms for a final concentration of 300 mg metal/L ARE. In situ biofilm formation supported by wicking ARE through the fiber lumen was observed by AFM imaging.

Analysis of Bacterial Growth. Serial dilutions were made of the planktonic cell cultures in the well plates using sterile DDI water and samples plated on LB plates with a 2% agar content. After 2 days growth at room temperature, colonies were counted and CFU/mL determined. For biofilm CFUs, the HFMs were harvested at 4 days and gently rinsed twice by immersion into sterile DDI water for 15 s. A 1 cm section of the HFM was cut and transferred to a bullet tube containing 1 mL of sterile DDI water and vortexed for 30 s at 1800 rpm (Fisher Scientific). Serial dilutions of the cells released from the HFM were made and plated onto LB agar to determine CFU/cm HFM.

Assessment of Biofilm Cell Density. Biofilm evolution was measured on HFMs cultured in ARE B for 6 days with sampling every 24 h. The influence of ARE C and N content was determined for HFMs cultured for 4 days in ARE B, ARE B(+gly), ARE B(+cit), ARE B(+gly+cit). CFUs were determined as described above.

Contact Angle Analysis. The hydrophobicity of the surfaces of native HFM, ARE B conditioned HFMs, and 6 days wheat roots were characterized by water contact angle analysis using a VCA-Optima-XE surface analysis system (AST Instruments, Bakersfield, CA). DDI water droplets (0.25 μL, n = 20) were deposited on flattened HFM fibers or fresh roots affixed to glass slides with double-sided tape.

SEM and EDS Analyses. SEM was performed with a FEI Quanta FEG 650 equipped with an Oxford X-Max energy dispersive X-ray spectroscope (EDS) housed in the Microscopy Core Facility at Utah State University. Samples were imaged under fixed and unfixed conditions between 0.3−0.5 Torr (low vacuum) with 10−14 kV accelerating potential without conductive coatings. Unfixed samples were rinsed twice by submersion in sterile DDI water and dried over 2 days at ambient conditions in covered Petri dishes. For fixation, rinsed samples were submerged in anhydrous methanol for 10 min and transferred into anhydrous ethanol twice for 30 min before immediate transfer for critical point dehydration with liquid CO_2 using a Tousimis Autosamdri 931 supercritical point drying apparatus.

AFM Imaging. Samples were imaged using a Digital Instruments Bioscope NSIIIa AFM in tapping mode with a Budget Sensors BSTap300 Al-coated cantilever. Bacterial lawn controls were prepared by scraping colonies from agar growth plates onto glass slides followed by immediate imaging. Real-time imaging of biofilm development on the HFM was recorded while wicking ARE through the fiber lumen.

Statistical Analysis. All samples were replicated at least three times and data are reported as means with standard deviation. A two-way ANOVA test with pairwise comparisons of treatment groups using REGWQ was performed on all well plate assay experiment data using the statistical program, SAS University Edition.

RESULTS AND DISCUSSION

Rhizoexudates and Bacterial Growth. Rhizoexudation is the key process feeding soil microbes and promoting microbial root colonization. Exudate released from a fresh wheat root harvested at 7 days after planting in a sand growth matrix is visualized as a viscous deposit released from the root onto the glass slide (Figure 2A); high-resolution AFM analysis of the

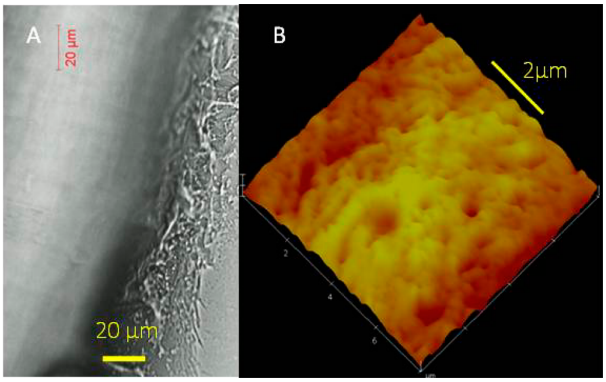

Figure 2. Rhizoexudation from wheat: brightfield (A) and AFM (B) images of wheat root exudate produced near root tip. Root harvested from 7 days-old wheat seedlings grown in a sand growth matrix.

root reveals a layer of exudates covering the root surface that obscures cell wall structure (Figure 2B). These exudates provide carbon and nitrogen sources that promote microbial growth as has been demonstrated for the beneficial pseudomonad, *Pc*O6.[24] The extensive colonization of a root from a *Pc*O6-inoculated wheat seed grown in sand and transferred to a LB growth plate is shown in Figure 3A. Colonies exhibit a characteristic orange color due to production of phenazines from *Pc*O6 cells.[13] SEM analysis of the root hair

DOI: 10.1021/acs.jafc.7b02524
J. Agric. Food Chem. 2018, 66, 6619−6627

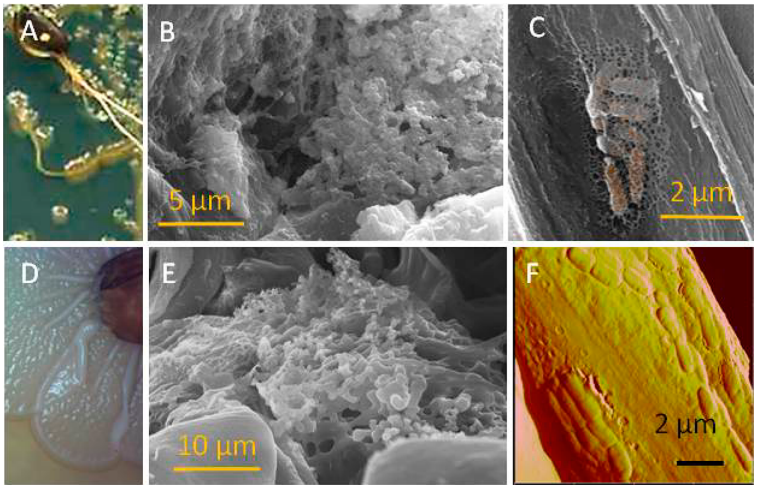

Figure 3. Bacterial colonization of wheat roots. (A) *Pc*O6 colony formation from inoculated wheat seedling on an ARE A (LB) growth plate. SEM images of a *Pc*O6 on the wheat root (B), and a root hair (C). (D) *Bs*309 endophyte emerging from a wheat seed on ARE A agar growth plate. (E) SEM image of *Bs*309 biofilm on the radicle. (F) AFM image of a root hair on a 7 day-old wheat seedling root showing *Bs*309 colonies. Samples fixed in methanol and critical point dried for SEM. AFM imaging of unfixed, hydrated sample.

zone reveals thick and layered biofilms. In some regions, copious extracellular polymeric substance (EPS) is produced, obscuring the bacterial cells (Figure 3B). On root hairs, individual cells are observed (Figure 3C), attached as a microcolony enmeshed in a thin EPS layer. *Pc*O6 is an aggressive and beneficial root colonizer, outcompeting other microbes on the root surface. The endophyte, isolate *Bs*309 (Figure 3D) also forms biofilms on the surface of the germinating root, the radicle (Figure 3E), as well as root hairs (Figure 3F). Both microbes are investigated here for colonization potential of the proposed root mimetic in order to understand responses in the biofilm to artificial root exudate (ARE) composition as well as abiotic stress of NPs without contributions from active plant metabolism. Thus, these rhizobacteria form a patchy, heterogeneous biofilms along the root surface (Figure 3C,F), colonizing intersections formed by lateral roots as well as the grooves formed where cells meet. Surface topography cues are evident in the microbial colonization observed in Figure 3F, where *Bs*309 cells align along the length of a hydrated root hair. Differences in exudation and water content are also observed between lateral roots and root hairs,[35] which contribute to a heterogeneous distribution of microbes in the rhizosphere.

Hollow Fiber Membrane as a Root Mimetic. SEM images of the four fiber types are shown in Figure 4, where it is noted that the PS/PVP and bleached PS/PVP surfaces are similar (Figure 4A,B), exhibiting pores, or "macrovoids" that form the outer surface of the HFM. Compared to the PS/PVP and bleached PS/PVP, the pure PS HFM exhibits greater relief in the form of thin (<1 μm) tendrils extending from the surface (Figure 4C, inset). The CD fiber exhibits a relatively uniform surface (Figure 4D), devoid of any visible pores. The measured macrovoid diameters on the PS/PVP (native and bleached) and PS fibers are similar in size (Table 1) to the lengths (1−2 μm) of the *Pc*O6 and *Bs*309 bacterial cells. Figure S1 shows *Pc*O6 and *Bs*309 cells adherent to the outermost surfaces of the bleached PS/PVP HFM.

The MW cutoff for all the HFMs is below 60 kDa; thus, the surface pores do not allow transport of bacteria into the fiber lumen, and microbes remain confined to the HFM surfaces, including on/within the pores, which provide anchoring points. The HFM root-mimetic, however, is homogeneous in terms of surface properties, allowing a focus of colonization in response

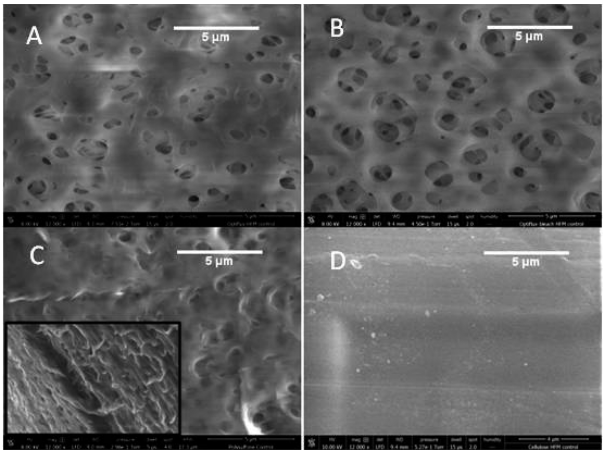

Figure 4. SEM images of HFM surfaces: (A) PS/PVP, (B) PS/PVP bleach-treated, and (C) PS. The inset image is taken at an angle to the surface to reveal the tendril-like structures normal to the surface. (D) Cellulose diacetate.

Table 1. HFM Surface Properties

external surface	macrovoid diameter[a] (μm)	SD (μm)	contact angle[b] (deg)	SD (deg)
PS/PVP	1.02	0.44	68.3	5.5
PS/PVP bleach treated	1.36	0.58	74.7	6.5
polysulfone (PS) only	0.97	0.25	72.4	4.9
cellulose diacetate (CD)	N/A	N/A	86.8	7.2
fresh 6 day wheat root	N/A	N/A	60.5	8.8
conditioned PS/PVP bleach treated	N/A	N/A	64.3	2.5

[a]Diameters are the mean of all macrovoids in a 15 μm × 15 μm image size for each fiber. [b]Contact angle values are the mean of 40 measurements.

DOI: 10.1021/acs.jafc.7b02524
J. Agric. Food Chem. 2018, 66, 6619−6627

to ARE composition variations to better understand the influence of root exudates on biofilm formation.

Surface Characterization and Affinity of the Rhizobacteria. The HFMs were characterized by their hydrophobicity, as measured from the water contact angles on fiber surfaces and compared with water contact angles measured on a fresh wheat root (Table 1). All of the fibers have contact angles less than 90° and are readily wet by the water droplet. Native PS/PVP (68.3°) becomes slightly more hydrophobic upon bleach treatment (74.7°), which is attributed to PVP chain scission and a reduction in PVP content in the fibers.[36] Conditioning of the fibers with a minimal medium artificial root exudate (ARE B) prior to measuring water contact angle yields a more hydrophilic surface (Table 1). The water contact angle was 64.3° for the ARE-conditioned PS/PVP bleach-treated HFM, close to the contact angle of 60.5° measured for a fresh 7 day wheat root.

The four HFMs were tested for bacterial affinity based on growth on the HFM immersed in ARE A for 24 h, as shown in Figure 5. Isolate *Bs*309, had significantly lower affinity for the HFM surfaces than the root surface colonizer, *Pc*O6. *Bs*309 remained in the 0.3−7 × 10^3 CFU/cm range where *Pc*O6 CFUs were in the 0.6−2 × 10^7/cm (Figure 5A). The stronger surface colonizing behavior of *Pc*O6 on the HFMs may reflect its lifestyle in the rhizosphere where it is found adhering to wheat root surfaces. Less is known about the *Bs*309−wheat interaction. Indeed, part of the benefit of the HFM root-mimetic is that the same abiotic surface is presented to all bacteria under investigation and the role of the plant host is restricted to selected ARE compositions.

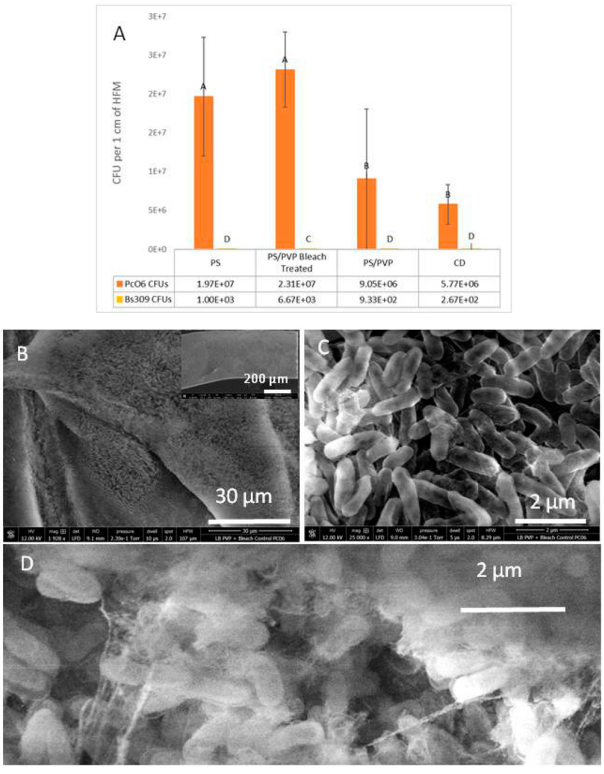

Figure 5. Assessment of HFM fibers for biofilm formation. (A) CFU comparison of culturable bacterial cells released from HFM surfaces after 24 h growth in LB (ARE A). (B−D) SEM images of mature biofilms formed on the PS/PVP bleach-treated fiber imaged after 4 days growth. Inset in part B is the low magnification image of colonized HFM. Samples imaged under low vacuum after methanol fixation and critical point drying.

HFM and Biofilm Formation. There are five major steps for biofilm formation: (1) reversible attachment of planktonic bacteria to a conditioned surface; (2) irreversible attachment of bacterial cells to the surface through adhesive appendages (pili)/surface proteins, cell aggregation, and production of EPS, such as alginate; (3) growth of colonies into early biofilm architectures; (4) biofilm maturation to form complex 3-D architectures, through increasing production and diversity of the EPS polymers to embed the cells; and (5) programmed release of cells. The physiochemical properties of the PS/PVP bleach-treated HFM were the most favorable to surface colonization (Figure 5A) and was, thus, selected as the fiber of choice for the biofilm analysis as a root-mimetic. SEM analysis of this fiber after 4 days of biofilm growth revealed a *Pc*O6 biofilm with extensive 3-D architecture (Figure 5B) that is indicative of a stage-4 biofilm. *Pc*O6 cell outlines are visible within the thick 4-day macrostructure. At higher magnification (Figure 5C,D), thread-like structures between cells are revealed that are possibly type IV pili and/or EPS.

Attachment of *Pc*O6 cells to an abiotic surface and to each other as the biofilm matures is likely to involve several bacterial surface traits. Attachment for other pseudomonads is correlated with flagella, type IV pili, and large surface proteins called Lap proteins.[37−39] Lap proteins may also function in cell-to-cell attractions required for biofilm maturation.[38] Flagella are observed on *Pc*O6 cells adsorbed on the PS/PVP-bleached HFM (Figure S1); as flagella aid in cell movement across surfaces,[38] they may participate in maturation of the biofilm through cell−cell interactions. The genome of *Pc*O6 contains genes encoding type IV pili. Two identified gene clusters are PchlO6_5320 *pilA*, PchlO6_5321 *pilC*, and PchlO6_5321 *pilD* and *pilM*, *pilN*, *pilP*, and *pilQ* at loci PchlO6_0450 to PchlO6_0453. PilQ is predicted to have a transport function.

*Pc*O6 also has the potential to make the adhesin, the Lap A protein. In *Pc*O6, the gene *lapA* (PchlO6_0139) is close to *lapD* (PchlO6_0137) and adjacent to a *tolC* family outer membrane transporter gene (PchlO6_0140), originally designated as *aggA* in a *P. putida* isolate, which when eliminated reduced root colonization ability.[40] LapA transport to the outer membrane protein allows it to act as an adhesin. This transport process is regulated by LapD, a cytoplasmic membrane spanning protein, that is intimately linked with biofilm formation through possessing a di-GMP binding site on the cytoplasmic domain.[41] Biofilms form with pseudomonads when the c-di-GMP levels rise, through processes that are highly regulated including nutrient availability.[38]

The effects of nutrients on formation of biofilms on the HFM were investigated using the chemically defined medium, ARE B, where carbon is supplied as citrate and sucrose and ammonium ions are the source of N, to better mimic nutrients available in the rhizosphere (Figure 6). As shown in the CFU graph in Figure 6A, *Pc*O6 growth as both the planktonic and biofilm forms peaked around day 3 with a decline from day 4 onward. Imaging biofilm formation with time through SEM was performed without chemical fixation (Figure 6B,C). A thin and sparse biofilm forms by day 1. The surface coverage increases and by day 3 has matured into layered structures. By day 5, more confluent biofilm coverage is observed on the HFM surface. No discernible changes were observed for biofilms on

DOI: 10.1021/acs.jafc.7b02524
J. Agric. Food Chem. 2018, 66, 6619−6627

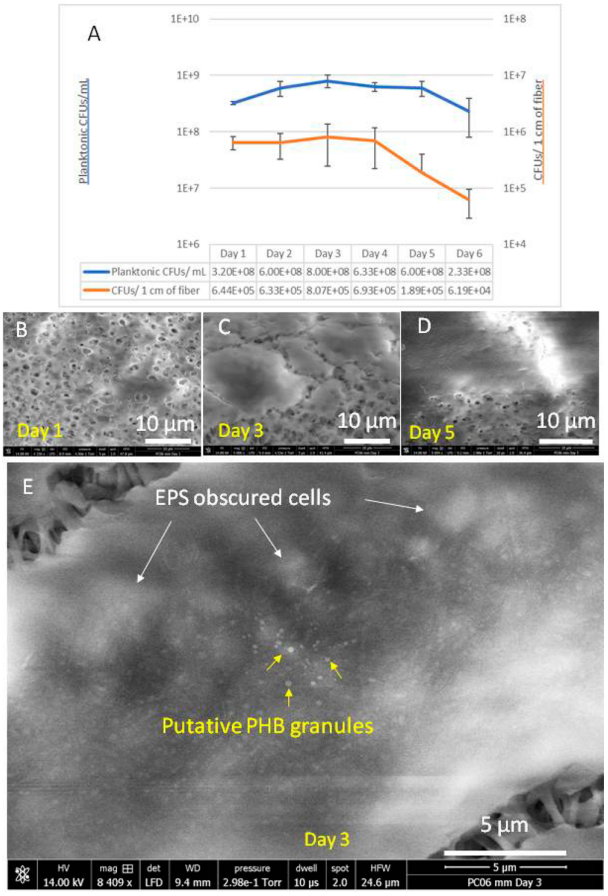

Figure 6. *Pc*O6 biofilm growth over time using minimal medium (ARE B) and PS/PVP bleach treated HFMs. (A) CFUs recovered from fiber are compared with CFUs from planktonic *Pc*O6 growth in the ARE. (B–D) SEM images of fibers harvested at 1, 3, and 5 days. (E) A higher magnification image of 3 day biofilm showing copious EPS layer overlaying cells and presence of putative PHB granules. SEM images collected without chemical fixation of samples.

fibers harvested on day 6 (not shown). A higher magnification SEM image of the biofilm (Figure 6C) reveals the outline of *Pc*O6 cells within a highly mucoid EPS layer. The bacterial cells also display round inclusions which may be polyhydroxybutyrate (PHB) granules. An *in situ* assessment of biofilm formation (Figure S2) reveals possible EPS formation in real-time; however, putative PHB granules were not resolved as cellular structures with AFM.

The *Pc*O6 genome contains genes predicted to be involved in synthesis of this PHB C-storage product. Genes are clustered at loci PchlO6_0432 to PchloO6_0438. The gene *phaD* at locus PchlO6_0435 is predicted to encode a regulator and *phaA* (PchlO6_0438) and *phaC* (PchlO6_0436) are annotated as encoding polymerases. This gene sequence is similar to the cluster responsible for PHB synthesis in *P. putida* KT2440. PHB synthesis in *P. putida* KT2440 is driven by low nitrogen high carbon growth. Glycerol is a frequently used carbon source in studies to optimize PHB production under chemostat conditions because it readily supplies the acetyl CoA required for synthesis of the polymer.[42]

Effects of Added Glycine and Citrate in the ARE on Biofilm Formation. To assess factors influencing granule formation and to understand how root-colonizing biofilm architecture varies with changes in root exudate composition, ARE-B was modified by addition of glycine, extra citrate, or both as defined in Table S1. Both glycine and citrate are found in rhizoexudates and pore waters.[32,43] Citrate is interesting because this metal chelator, along with malate, increases in concentration upon challenge of wheat with Cu and Al ions.[44] Thus, correlating how ARE nutrient supplies influence biofilm growth on the root-mimetic HFM provides a model to understand bacteria growth in the rhizosphere.

Figure 7A shows the 4 day CFUs from fibers, contrasted with CFUs from planktonic cultures for increased ARE B(+cit), ARE

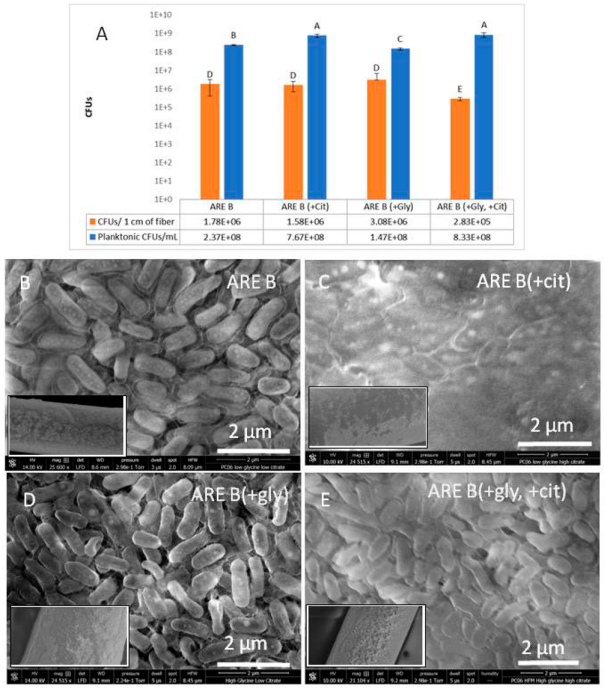

Figure 7. Changes in *Pc*O6 biofilm and planktonic CFUs in minimal medium (ARE B) with and without added glycine (ARE B + gly) and citrate (ARE B + cit). (A) CFU counts were taken after 4 days of growth. (B–C) Granule formation clearly observed for ARE B as well ARE B(+cit); however, in panel C the cells are more obscured by EPS, presumably produced in response to additional citrate. (D) Cells grown on ARE(+gly), a second nitrogen source, produce less visible granules than those shown in panels B and C. Cells also are clearly visible suggesting reduced EPS production. (E) Increasing citrate in the presence of glycine appears to partially restore EPS production. Granule formation is also not noted, but somewhat obscured by EPS, and attributed to the glycine as a second source of N. Low magnification images of corresponding HFMs are shown in the insets of each panel. Additional images of *Pc*O6 granules (ARE B) and partial restoration of EPS in ARE B(+gly + cit) are shown in Figure S3. All samples were fixed in methanol and critical point dried prior to SEM imaging.

B(+gly), in comparison with ARE B. Fibers were analyzed on day 4 to allow for biofilm maturity. The SEM images are of samples that were chemically fixed using methanol, which produced better imaging of the cells through dehydration of cellular and extracellular materials. This is noticed when comparing the cells grown in ARE B in Figure 6 to those in Figure 7. In Figure 6, the unfixed cells are obscured within a

DOI: 10.1021/acs.jafc.7b02524
J. Agric. Food Chem. 2018, 66, 6619–6627

thick mucoidal layer, while after chemical fixing in methanol (Figure 7) cell outlines are revealed and the putative PHB granules are clearly discernible within the microbial cells.

Only the biofilms formed with growth on ARE B(+cit) (Figure 7) displayed a thick layered structure that showed cracking upon fixation, although value of the CFUs recovered from the 4 day biofilm were not different from the ARE B- biofilms. With additional citrate, the bacterial cells appear more tightly packed and are obscured by a cohesive mucoid EPS layer (Figure 7C vs Figure 7B). Granules are present within the cells grown on both ARE B and ARE B(+cit) but are less discernible in the latter, perhaps due to the overlay of EPS. EPS production by root-colonizing bacteria may benefit the host plant as the biofilm forms a matrix covering root cells that may retain water, chelate micronutrients and protect against pathogens.

The *Pc*O6 EPS composition is unknown but likely includes alginate. For *Pc*O6, a large gene cluster associated with alginate synthesis is located between Pchl_0107 and Pchl_1029 and regulatory genes at other locations are present. Alginate production in other microbes is intimately linked with regulation at the transcriptional and translation levels by c-di GMP for cells to switch to a biofilm lifestyle.[45] The predicted sequence, *algA*, *algF*, *algJ*, *algI*, *algL*, *algX*, *alg G*, *algE*, *algK*, *alg44*, *alg8*, and *algD*, is identical to those found in *P. syringae* and *P. aeruginosa*, and similarly, additional genes that function as regulators[46] are located elsewhere on the chromosome. The finding that alginate is stimulated by Cu and osmotic stress in *P. syringae*[46] and by Zn[47] in *P. putida* suggests that the gene array is likely to be activated in *Pc*O6 by interactions with CuO and ZnO NPs and/or released ions. Future work will focus on generating mutants in alginate production and assess mutant colonization and biofilm formation on the HFM root mimetic.

The ARE containing glycine, ARE B(+gly) provides a different nitrogen source in addition to the ammonium ions in ARE B or ARE B(+cit), an addition that may free up metabolism to produce more N-containing structures such as Lap proteins/pili, as described previously. The network of thread-like structures interconnecting the cells grown on ARE B(+gly) (Figure 7D) may contain more N than those formed on nonglycine ARE B media. Interestingly, the EPS formation for biofilms grown on glycine containing ARE is partially restored when citrate concentration is doubled, ARE B(+gly + cit), Figure 7E. Surprisingly, despite provision of more N, this biofilm had the fewest recoverable CFUs (Figure 7A). However, this may result from a more cohesive biofilm that releases fewer cells during CFU assessment.

Effects of NPs on HFM Biofilms. Having demonstrated the suitability of the PS/PVP-bleached HFM for hosting biofilms nourished with AREs, we applied this platform to assess the response of the ARE B-fed biofilms to NP challenges. CuO and ZnO NPs are selected as representative of agriculturally relevant NPs, with potential to serve as fertilizers or, at higher doses, pesticides. Previous work[31,32] shows that growth of wheat or bean seedlings for 7 days in the presence of either CuO or ZnO NPs did not affect colonization of *Pc*O6, as determined as culturable cells released from excised roots; however, these NPs stressed bacterial growth and caused differences in biofilm formation. Figure 8 reveals NP effects on *Pc*O6 biofilms formed on the HFM. The CuO and ZnO NPs were introduced at 300 mg/L of ARE B, and were either added at the same time as the inoculum (0 h) or 3 days after inoculation to allow biofilms to be already established prior to

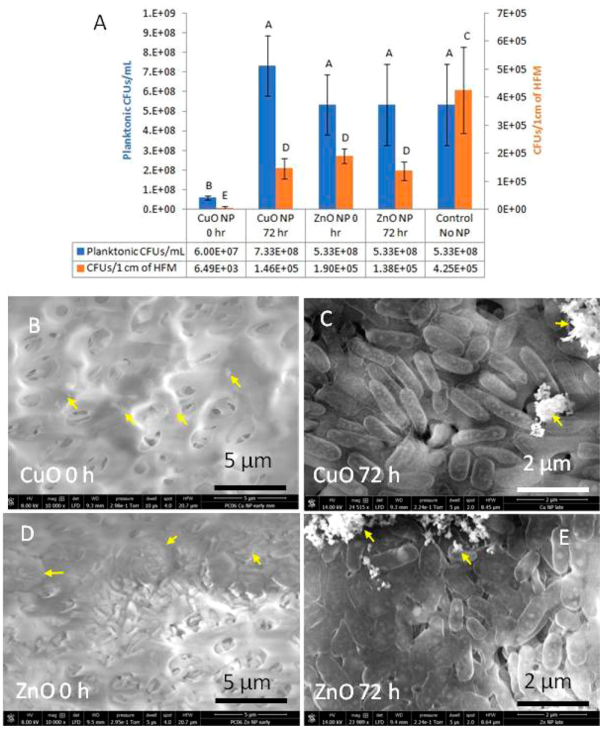

Figure 8. ZnO and CuO NP challenges to *Pc*O6 biofilms on the root mimetic HFM with ARE B medium. All samples were removed from the culture at 96 h, and the NP challenges were either introduced at initiation (0 h) or 72 h after initiation. (A) *Pc*O6 planktonic and biofilm response to 300 mg/L CuO and ZnO NP challenges. (B–E) SEM images of methanol fixed and critical point dried biofilms challenged with CuO NPs at time of inoculation (B) or after 72 h growth (C) or ZnO NPs at time of inoculation (D) or after 72 h growth (E). NPs and aggregates indicated by arrows. EDS maps of CuO and ZnO shown in Figures S4 and S5.

the NP stress. The data show that both treatment regimens and both NPs significantly reduced the biofilm CFUs compared with the NP-free control (Figure 8A). All CFU and SEM analysis were obtained 4 days postinoculation. The most significant CFU reduction was observed with CuO NPs introduction at time zero (6.5×10^3 CFU/cm), which was a two-log CFU reduction compared to the NP-free control (4.3×10^5 CFU/cm). When CuO NPs were added to established biofilms at 3 days, a modest reduction in CFUs was measured 24 h later (1.5×10^5 CFU/cm). SEM analysis of the root mimetic when challenged with CuO NP at time zero (Figure 8B,C) revealed an absence of biofilm, although individual microbes and small aggregates were observed. For CuO NPs delivered at 3 days, the biofilm appeared less structured than the unchallenged biofilm (e.g., Figure 7B). EDS analysis (Figure S4) identified the particles and aggregates as containing both Cu and O.

The ZnO NPs, either when introduced at time zero or 3 days, reduced recoverable CFUs ($1.4–1.9 \times 10^5$ CFU/cm) as compared with the biofilm from the NP-free control (4.3×10^5 CFU/cm). Unlike CuO NPs, the ZnO NPs yielded no significant CFU difference between the two introduction times for either biofilm or planktonic *Pc*O6. *Pc*O6 has higher toxicity threshold to ZnO NPs and released ions than it does to CuO NPs/ions, and the dose, 300 mg metal oxide/L, is sublethal. SEM analysis supports the lower toxicity of ZnO NPs

DOI: 10.1021/acs.jafc.7b02524
J. Agric. Food Chem. 2018, 66, 6619–6627

compared to CuO NPs, revealing confluent microbial colonies as well as individual adherent microbes for the ZnO challenged root mimetic (Figure 8D,E). For the ZnO challenged biofilms an EPS layer was not observed, and the thread-like structures seen interconnecting cells on ARE B were also missing. Putative PHB granules were still observable for the ZnO NP challenged cells (Figure 8E). EDS analysis (Figure S5) identified the particles and aggregates as ZnO. For both NP challenges, the bacterial cells appear more elongated than the controls. Measuring the cell sizes (Figure S6) reveals cell lengths ranging from 0.7−1.2 μm for control cells, 0.9−1.6 μm for ZnO NP challenges, and 0.9−1.9 μm for CuO NP challenges, perhaps due to induced reactive oxygen stress.

In summary, the root-mimetic HFM permits exploration of NP−biofilm interactions under controlled conditions where rhizoexudates are maintained with a constant defined composition using AREs. In contrast to *Bs*309, *Pc*O6 formed extensive biofilms on the hollow fiber root mimetic under the conditions investigated. CuO NP challenges diminished *Pc*O6 biofilm forming ability when delivered prior to biofilm establishment whereas ZnO NPs were not inhibitory to *Pc*O6 biofilm formation. Both CuO and ZnO NP exposure resulted in larger bacteria. The most prominent effect of altered ARE composition was production with increased citrate of a cohesive mucoid EPS coating the biofilm. Intracellular granule formation was observed for all biofilms. We speculate, based on the existing literature, that these granules contain PHB produced as a storage product when C is in excess. The PHB are transitory being degraded when needed. Consequently, these storage granules could benefit the bacteria when plants are nutrient stressed, such as in the diurnal cycle when C supply to the root is diminished. The prolonged activity of the root microbiome may in turn benefit the plant. These findings have implications in agricultural use, as they suggest that these metal oxide NPs at the investigated concentrations would have a minimal impact on preformed biofilms but could delay the initiation of biofilms if NPs accumulated in the soils. In addition, the entrapment of NPs into the biofilm cells and on plant root surfaces including root hairs[48] and exudate could be part of the mechanisms involved in cross-kingdom transfer of NPs as entry points into the food chain.[49] The rhizosphere contains many organisms that graze on plant roots so that they would ingest the NPs.[50] NP-rhizosphere processes, as outlined in Figure 1, are a complex interplay of plant-microbe-NP-and soil pore water factors. The root mimetic HFM allows for a serial assessment of each component, with nutrition to mimic root exudates or soil pore water being user-defined AREs. The production of putative PHB granules by *Pc*O6 biofilms may allow them to withstand stresses arising when the plant produces fewer exudates as well as possibly to NP exposure by providing an internal carbon source. Increased EPS production by the *Pc*O6 biofilm fed an artificial exudate with twice the citrate will be explored in future NP studies to assess the relationship between EPS and free citrate activities on the NPs.

■ ASSOCIATED CONTENT

Supporting Information

The Supporting Information is available free of charge on the ACS Publications website at DOI: 10.1021/acs.jafc.7b02524.

Artificial root exudate recipes, SEM with EDS analysis of NP-challenged biofilms, bacteria morphology and histograms of NP-induced changes in bacteria sizes, and real-time AFM of biofilm growth (PDF)

■ AUTHOR INFORMATION

Corresponding Author

*Phone: 435 797 2158. E-mail: david.britt@usu.edu.

ORCID

Anne Anderson: 0000-0002-0463-2174

David W. Britt: 0000-0002-9753-6404

Funding

Funding from the USU AES station, Project 1280, Grants AFRI USDA-NIFA 2016-08771, NSF CBET 1705874 and SEM instrumentation NSF Grant CMMI 1337932 are gratefully acknowledged.

Notes

The authors declare no competing financial interest.

■ ACKNOWLEDGMENTS

SEM training through the USU Core Microscopy Facility and training of students by Fen-Ann Shen is very much appreciated.

■ REFERENCES

(1) Bakker, P.; Berendsen, R.; Doornbos, R.; Wintermans, P.; Pieterse, C. The rhizosphere revisited: root microbiomics. *Front. Plant Sci.* **2013**, *4*, 1−7.

(2) Pérez-Jaramillo, J. E.; Mendes, R.; Raaijmakers, J. M. Impact of plant domestication on rhizosphere microbiome assembly and functions. *Plant Mol. Biol.* **2016**, *90*, 635−644.

(3) Rouatt, J.; Katznelson, H. A study of the bacteria on the root surface and in the rhizosphere soil of crop plants. *J. Appl. Bacteriol.* **1961**, *24*, 164−171.

(4) Fischer, H.; Meyer, A.; Fischer, K.; Kuzyakov, Y. Carbohydrate and amino acid composition of dissolved organic matter leached from soil. *Soil Biol. Biochem.* **2007**, *39*, 2926−2935.

(5) Lesuffleur, F.; Paynel, F.; Bataillé, M.-P.; Le Deunff, E.; Cliquet, J.-B. Root amino acid exudation: measurement of high efflux rates of glycine and serine from six different plant species. *Plant Soil* **2007**, *294*, 235−246.

(6) Barber, D. A.; Martin, J. K. The release of organic substances by cereal roots into soil. *New Phytol.* **1976**, *76*, 69−80.

(7) Hutsch, B. W.; Augustin, J.; Merbach, W. Plant rhizodeposition-an important source for carbon turnover in soils. *J. Plant Nutr. Soil Sci.* **2002**, *165*, 397.

(8) Lareen, A.; Burton, F.; Schäfer, P. Plant root-microbe communication in shaping root microbiomes. *Plant Mol. Biol.* **2016**, *90*, 575−587.

(9) Ramey, B. E.; Koutsoudis, M.; von Bodman, S. B.; Fuqua, C. Biofilm formation in plant−microbe associations. *Curr. Opin. Microbiol.* **2004**, *7*, 602−609.

(10) Timmusk, S.; El-Daim, I. A. A.; Copolovici, L.; Tanilas, T.; Kännaste, A.; Behers, L.; Nevo, E.; Seisenbaeva, G.; Stenström, E.; Niinemets, Ü. Drought-tolerance of wheat improved by rhizosphere bacteria from harsh environments: enhanced biomass production and reduced emissions of stress volatiles. *PLoS One* **2014**, *9*, e96086.

(11) Berendsen, R. L.; Pieterse, C. M.; Bakker, P. A. The rhizosphere microbiome and plant health. *Trends Plant Sci.* **2012**, *17*, 478−486.

(12) Yang, J.; Kloepper, J. W.; Ryu, C.-M. Rhizosphere bacteria help plants tolerate abiotic stress. *Trends Plant Sci.* **2009**, *14*, 1−4.

(13) Spencer, M.; Ryu, C.-M.; Yang, K.-Y.; Kim, Y. C.; Kloepper, J. W.; Anderson, A. J. Induced defence in tobacco by *Pseudomonas chlororaphis* strain O6 involves at least the ethylene pathway. *Physiol. Mol. Plant Pathol.* **2003**, *63*, 27−34.

(14) Chung, J.-h.; Song, G. C.; Ryu, C.-M. Sweet scents from good bacteria: case studies on bacterial volatile compounds for plant growth and immunity. *Plant Mol. Biol.* **2016**, *90*, 677−687.

DOI: 10.1021/acs.jafc.7b02524
J. Agric. Food Chem. 2018, 66, 6619−6627

(15) Dimkpa, C. O.; McLean, J. E.; Latta, D. E.; Manangón, E.; Britt, D. W.; Johnson, W. P.; Boyanov, M. I.; Anderson, A. J. CuO and ZnO nanoparticles: phytotoxicity, metal speciation, and induction of oxidative stress in sand-grown wheat. *J. Nanopart. Res.* **2012**, *14*, 1125−1139.
(16) Jin, C. W.; Ye, Y. Q.; Zheng, S. J. An underground tale: contribution of microbial activity to plant iron acquisition via ecological processes. *Ann. Bot. (Oxford, U. K.)* **2014**, *113*, 7−18.
(17) Reid, A.; Greene, S. E. *How Microbes Can Help Feed the World*, Report on an American Academy of Microbiology Colloquium, Washington, DC , December 2012, American Academy of Microbiology: Washington, DC, 2013; pp 33−37.
(18) Timmusk, S.; Behers, L.; Muthoni, J.; Muraya, A.; Aronsson, A.-C. Perspectives and challenges of microbial application for crop improvement. *Front. Plant Sci.* **2017**, *8*, 1−10.
(19) DeRosa, M. C.; Monreal, C.; Schnitzer, M.; Walsh, R.; Sultan, Y. Nanotechnology in fertilizers. *Nat. Nanotechnol.* **2010**, *5*, 91−91.
(20) Zahra, Z.; Arshad, M.; Rafique, R.; Mahmood, A.; Habib, A.; Qazi, I. A.; Khan, S. A. Metallic nanoparticle (TiO_2 and Fe_3O_4) application modifies rhizosphere phosphorus availability and uptake by *Lactuca sativa*. *J. Agric. Food Chem.* **2015**, *63*, 6876−6882.
(21) Raliya, R.; Tarafdar, J. C.; Biswas, P. Enhancing the mobilization of native phosphorus in the mung bean rhizosphere using ZnO nanoparticles synthesized by soil fungi. *J. Agric. Food Chem.* **2016**, *64*, 3111−3118.
(22) Wang, Z.; Xie, X.; Zhao, J.; Liu, X.; Feng, W.; White, J. C.; Xing, B. Xylem-and phloem-based transport of CuO nanoparticles in maize (*Zea mays* L.). *Environ. Sci. Technol.* **2012**, *46*, 4434−4441.
(23) Goodman, J.; Mclean, J. E.; Britt, D. W.; Anderson, A. J. Sublethal doses of ZnO nanoparticles remodel production of cell signaling metabolites in the root colonizer *Pseudomonas chlororaphis* O6. *Environ. Sci.: Nano* **2016**, *3*, 1103−1113.
(24) Martineau, N.; McLean, J. E.; Dimkpa, C. O.; Britt, D. W.; Anderson, A. J. Components from wheat roots modify the bioactivity of ZnO and CuO nanoparticles in a soil bacterium. *Environ. Pollut. (Oxford, U. K.)* **2014**, *187*, 65−72.
(25) Mah, T.-F. Biofilm-specific antibiotic resistance. *Future Microbiol.* **2012**, *7*, 1061−1072.
(26) Housley, L.; Anderson, T.; Sontag, N.; Han, S.-H.; Britt, D. W.; Anderson, A. J. Pluronics' influence on pseudomonad biofilm and phenazine production. *FEMS Microbiol. Lett.* **2009**, *293*, 148−153.
(27) Redding, M.; Shorten, P.; Lewis, R.; Pratt, C.; Paungfoo-Lonhienne, C.; Hill, J. Soil N availability, rather than N deposition, controls indirect N_2O emissions. *Soil Biol. Biochem.* **2016**, *95*, 288−298.
(28) Ziegler, M.; Engel, M.; Welzl, G.; Schloter, M. Development of a simple root model to study the effects of single exudates on the development of bacterial community structure. *J. Microbiol. Methods* **2013**, *94*, 30−36.
(29) Watkins, A. J.; Nicol, G. W.; Shaw, L. J. Use of an artificial root to examine the influence of 8-hydroxyquinoline on soil microbial activity and bacterial community structure. *Soil Biol. Biochem.* **2009**, *41*, 580−585.
(30) Nichols, D.; Cahoon, N.; Trakhtenberg, E.; Pham, L.; Mehta, A.; Belanger, A.; Kanigan, T.; Lewis, K.; Epstein, S. Use of ichip for high-throughput in situ cultivation of "uncultivable" microbial species. *Appl. Environ. Microbiol.* **2010**, *76*, 2445−2450.
(31) Dimkpa, C. O.; McLean, J. E.; Britt, D. W.; Anderson, A. J. Nano-CuO and interaction with nano-ZnO or soil bacterium provide evidence for the interference of nanoparticles in metal nutrition of plants. *Ecotoxicology* **2015**, *24*, 119−129.
(32) Wright, M.; Adams, J.; Yang, K.; McManus, P.; Jacobson, A.; Gade, A.; McLean, J.; Britt, D.; Anderson, A. A root-colonizing pseudomonad lessens stress responses in wheat imposed by CuO nanoparticles. *PLoS One* **2016**, *11*, e0164635.
(33) Chen, Y.; Yan, F.; Chai, Y.; Liu, H.; Kolter, R.; Losick, R.; Guo, J. H. Biocontrol of tomato wilt disease by Bacillus subtilis isolates from natural environments depends on conserved genes mediating biofilm formation. *Environ. Microbiol.* **2013**, *15*, 848−864.
(34) Madsen, B.; Britt, D. W.; Griffiths, F.; McKenna, E.; Ho, C. H. Effect of sterilization techniques on the physicochemical properties of polysulfone hollow fibers. *J. Appl. Polym. Sci.* **2011**, *119*, 3429−3436.
(35) Berg, G.; Smalla, K. Plant species and soil type cooperatively shape the structure and function of microbial communities in the rhizosphere. *FEMS Microbiol. Ecol.* **2009**, *68*, 1−13.
(36) Wienk, I.; Meuleman, E.; Borneman, Z.; Van Den Boomgaard, T.; Smolders, C. Chemical treatment of membranes of a polymer blend: mechanism of the reaction of hypochlorite with poly (vinyl pyrrolidone). *J. Polym. Sci., Part A: Polym. Chem.* **1995**, *33*, 49−54.
(37) Bennett, R. R.; Lee, C. K.; De Anda, J.; Nealson, K. H.; Yildiz, F. H.; O'Toole, G. A.; Wong, G. C.; Golestanian, R. Species-dependent hydrodynamics of flagellum-tethered bacteria in early biofilm development. *J. R. Soc., Interface* **2016**, *13*, 20150966.
(38) Fuqua, C. Passing the baton between laps: adhesion and cohesion in *Pseudomonas putida* biofilms. *Mol. Microbiol.* **2010**, *77*, 533−536.
(39) Barken, K. B.; Pamp, S. J.; Yang, L.; Gjermansen, M.; Bertrand, J. J.; Klausen, M.; Givskov, M.; Whitchurch, C. B.; Engel, J. N.; Tolker-Nielsen, T. Roles of type IV pili, flagellum-mediated motility and extracellular DNA in the formation of mature multicellular structures in *Pseudomonas aeruginosa* biofilms. *Environ. Microbiol.* **2008**, *10*, 2331−2343.
(40) Buell, C.; Anderson, A. Genetic analysis of the aggA locus involved in agglutination and adherence of *Pseudomonas putida*, a beneficial fluorescent pseudomonad. *Mol. Plant-Microbe Interact.* **1992**, *5*, 154−162.
(41) Navarro, M. V.; Newell, P. D.; Krasteva, P. V.; Chatterjee, D.; Madden, D. R.; O'Toole, G. A.; Sondermann, H. Structural basis for c-di-GMP-mediated inside-out signaling controlling periplasmic proteolysis. *PLoS Biol.* **2011**, *9*, e1000588.
(42) Beckers, V.; Poblete-Castro, I.; Tomasch, J.; Wittmann, C. Integrated analysis of gene expression and metabolic fluxes in PHA-producing *Pseudomonas putida* grown on glycerol. *Microb. Cell Fact.* **2016**, *15*, 73−90.
(43) Warren, C. R. Wheat roots efflux a diverse array of organic N compounds and are highly proficient at their recapture. *Plant Soil* **2015**, *397*, 147−162.
(44) Nian, H.; Yang, Z. M.; Ahn, S. J.; Cheng, Z. J.; Matsumoto, H. A comparative study on the aluminium-and copper-induced organic acid exudation from wheat roots. *Physiol. Plant.* **2002**, *116*, 328−335.
(45) Fata Moradali, M.; Donati, I.; Sims, I. M.; Ghods, S.; Rehm, B. H. Alginate polymerization and modification are linked in *Pseudomonas aeruginosa*. *mBio* **2015**, *6*, e00453-15.
(46) Penaloza-Vazquez, A.; Kidambi, S. P.; Chakrabarty, A. M.; Bender, C. L. Characterization of the alginate biosynthetic gene cluster in *Pseudomonas syringae* pv. syringae. *J. Bacteriol.* **1997**, *179*, 4464−4472.
(47) Mumm, K.; Ainsaar, K.; Kasvandik, S.; Tenson, T.; Hõrak, R. Responses of *Pseudomonas putida* to zinc excess determined at the proteome level: pathways dependent and independent of ColRS. *J. Proteome Res.* **2016**, *15*, 4349−4368.
(48) Adams, J.; Wright, M.; Wagner, H.; Valiente, J.; Britt, D.; Anderson, A. Cu from dissolution of CuO nanoparticles signals changes in root morphology. *Plant Physiol. Biochem.* **2017**, *110*, 108−117.
(49) Rico, C. M.; Majumdar, S.; Duarte-Gardea, M.; Peralta-Videa, J. R.; Gardea-Torresdey, J. L. Interaction of nanoparticles with edible plants and their possible implications in the food chain. *J. Agric. Food Chem.* **2011**, *59*, 3485.
(50) Bonkowski, M.; Villenave, C.; Griffiths, B. Rhizosphere fauna: the functional and structural diversity of intimate interactions of soil fauna with plant roots. *Plant Soil* **2009**, *321*, 213−233.

DOI: 10.1021/acs.jafc.7b02524
J. Agric. Food Chem. 2018, 66, 6619−6627